A phase-field model for simulating various spherulite morphologies of semi-crystalline polymers*

Wang Xiao-Dong(王晓东), Ouyang Jie(欧阳洁)†, Su Jin(苏 进), and Zhou Wen(周 文)

Department of Applied Mathematics, Northwestern Polytechnical University, Xi'an 710129, *China*

(Received 24 December 2012; revised manuscript received 26 March 2013)

A modified phase-field model is proposed for simulating the isothermal crystallization of polymer melts. The model consists of a second-order phase-field equation and a heat conduction equation. It obtains its model parameters from the real material parameters and is easy to use with tolerable computational cost. Due to the use of a new free energy functional form, the model can reproduce various single crystal morphologies of polymer melts under quiescent conditions, including dendritic, lamellar branching, ring-banded , breakup of ring-banded, faceted hexagonal, and spherulitic structures. Simulation results of isotactic polystyrene crystals demonstrate that the present phase-field model has the ability to give qualitative predictions of polymer crystallization under isothermal and quiescent conditions.

Keywords: phase-field, crystallization, polymer, dendritic, lamellar, ring-banded

PACS: 61.50.Ah, 81.30.–t **DOI:** 10.1088/1674-1056/22/10/106103

1. Introduction

As is well known, polymers have become some of the most important technical materials in our daily life. The properties and failure characteristics of polymeric products fabricated by freezing liquids into solids are to a great extent affected by their microstructures formed during solidification. Therefore, it is indispensable to establish a powerful numerical model that can predict these microstructures, especially the various crystallization morphologies of semi-crystalline polymers. And the predicted microstructures may supply a theoretical basis for controlling or optimizing the fabrication procedures.

Spherulites, which are usually formed under quiescent or low shear conditions, are the most common morphologies observed in polymeric solids. The term "spherulites" used here represents a class of crystals with nearly spherical shapes in a broader sense, including dendritic patterns,[1] lamellar branching patterns,[2] ring-banded patterns,[3] etc. Although phenomenal characteristics of spherulites have been clearly known from the experimental studies over the last decades, the specific mechanisms that lead to the formation of such intricate structures are usually poorly understood.[4] A possible approach to remedying the shortage of experimental studies searching for further mechanisms of such structures is to invoke mathematical modeling. Indeed, a number of phenomenological models[5–9] have been proposed for spherulite crystallizations. The most prevalent outcome of these models is the phase field theory. At present, the phase field theory has already demonstrated its ability to describe complex crystal morphologies.[10]

The phase field theory is a mathematical model for solving interfacial problems. Its basis is a partial differential equation for the evolution of an auxiliary field that is represented by an order parameter. Up to now, a number of phase field models[11–13] have been established based on various free energy functional forms depending on order parameters and other diffusive fields. One of the greatest successes of the phase field model is that it has been successfully applied to the dendritic crystal growth in metal alloys.[14] Recently, it has begun to be applied to polymer systems for modeling more complex crystal morphologies. The most representative contributions are those done by Gránásy *et al.*[4,10] and Xu *et al.*[15,16] Gránásy *et al.*[10] mainly focused on reproducing the entire range of observed spherulite morphologies by modifying the free energy functional form phenomenologically and adding other diffusive fields. They presented two phase field models[4,10] according to the earlier results by Warren and Boettinger[17] and Kobayashi *et al.*[18] And the models have been successfully used to simulate the polycrystalline growth morphologies in thin polymer films. Xu *et al.*[15,16] devoted their efforts to the establishment of phase field models having polymeric characteristics, where the model parameters can be evaluated directly from the experimentally measurable material parameters and the phase field order parameter has real physical meaning. A couple of such type phase field models, which are model A[15,19] for uniform polymer melts and model C[16] for polymer blends or nonuniform polymer melts, were presented by Kyu *et al.* according to the phase field model

*Project supported by the National Key Basic Research Program of China (973 Program) (Grant No. 2012CB025903), the Foundation for Fundamental Research of Northwestern Polytechnical University, China (Grant No. JCY20130141), the Doctorate Foundation of Northwestern Polytechnical University, China (Grant No. cx201019), and the Fund for Doctoral Students Newcomer Awards from the Ministry of Education of China.

†Corresponding author. E-mail: jieouyang@nwpu.edu.cn

© 2013 Chinese Physical Society and IOP Publishing Ltd

of Kobayashi[20] and the asymmetric free energy functional forms of Harrowell and Oxtoby.[21] By using these models, many simulation results have been obtained.

However, the phase field models proposed by both groups have their own imperfections. Models of Gránásy *et al.* used several artificially specified model parameters which are not evaluated from the real material parameters. This is not convenient for relating the simulation results to the experiments. In addition, the models each contain a fourth-order partial differential equation and several second-order partial differential equations with complex forms in two dimensions, and even more equations with more complex forms in three dimensions are involved. Thus, the models are not easy to use and the corresponding computational costs are huge. Moreover, the models cannot simulate the ring-banded structures. Model C of Kyu *et al.* also used some artificially specified model parameters, and has the problem of a high computational cost. The simulated morphologies obtained by model C are not richer than those simulated by Gránásy's models. Model A of Kyu *et al.* obtains its model parameters from the real material parameters and is very simple to use, but it has a severe scaling problem caused by the fact that the heat diffusion is much faster than the solute diffusion. For example, when the model is used to simulate the single crystals of isotactic polystyrene,[15] the dimensionless diffusion coefficient of the heat conduction equation is 65.8 (data from Ref. [15]) which results in a maximal dimensionless time step $\Delta\tau = 10^{-3}$ for stability reason ($1\tau = 10^{-5}$ s). For the results at the time $t = 66$ s (Fig. 3 in Ref. [15]), the number of the computational steps reach 6.6×10^9, which will cost at least 6.6×10^7 s CPU time (about two years) on an ordinary personal computer for a grid of 512×512. Huge computational cost may prevent model A from being widely used. Moreover, the model still cannot simulate the ring-banded structures.

In view of these problems, the primary objective of the present paper is to propose a powerful phase-field model to alleviate the existing difficulties. The new model can be viewed as a variant of Kyu's model A. It inherits the virtues of Kyu's model A, which includes obtaining its model parameters from the real material parameters and being very simple to use. Most importantly, it eliminates the scaling problem by using a virtual temperature field, which is obtained by slowing down the real heat conduction. Thus, the computational cost of the new model is greatly reduced. Moreover, it can simulate more microstructure patterns (including the ring-banded patterns) than Kyu's model A, owing to the use of a different free energy functional form.

The remainder of this paper is organized as follows. In Section 2 a powerful phase-field model is presented for simulating various spherulitic morphologies of a polymer system. In Section 3, several simulation results are shown and discussed. Finally, some brief conclusions are drawn in Section 4.

2. Theoretical model

The phase-field model uses an order parameter to describe the phase transition of a material. Values of the order parameter are usually limited between two specified values, which represent the amorphous state and stable crystal state, respectively. The evolution of the order parameter is governed by a non-conserved phase-field equation coupled with some evolution equations of physical quantities which have important effects on the crystallization, such as latent heat and blend concentration. In this work, the polymer melts considered are uniform, thus the change in the concentration caused by phase separation may be neglected. By contrast, the thermal conduction of latent heat is prominent and regarded as an important factor in polymer crystallization. Therefore, the modified phase-field model will consist of a non-conserved phase-field equation and a heat conduction equation. It improves Kyu's model A[15] by using a virtual temperature field to eliminate the scaling problem and a modified free energy functional form to eliminate some mathematical inconsistencies, and hence to simulate more microstructure patterns.

2.1. Phase-field equation

According to the Ginzburg–Laudau theory, the temporal evolution of the crystal order parameter can be modeled by the following non-conserved phase-field equation as

$$\frac{\partial \psi(\boldsymbol{x},t)}{\partial t} = -\Gamma \frac{\delta F(\psi,T)}{\delta \psi(\boldsymbol{x},t)}, \tag{1}$$

where $\psi(\boldsymbol{x},t)$ represents the crystal order parameter at time t and position $\boldsymbol{x}$; $\Gamma = D/d^2$ is the mobility which is inversely proportional to the viscosity of the melt, with d being the characteristic length for single crystals, D the diffusion coefficient; $F(\psi,T)$ is the total free energy of the freezing system, defined in terms of a combination of a local free energy density and a nonlocal gradient term as

$$\begin{aligned} F(\psi,T) &= \int f_{\text{cryst}}(\psi,T)\,\mathrm{d}V \\ &= \int [f_{\text{local}}(\psi,T) + f_{\text{grad}}(\psi)]\,\mathrm{d}V, \end{aligned} \tag{2}$$

with T being the temperature, $f_{\text{local}}(\psi,T)$ and $f_{\text{grad}}(\psi)$ the local free energy density and the nonlocal free energy density, respectively.

As is well known, it is hard to fully crystallized the crystalline polymer melts. Therefore, various metastable states of defective polymer crystals should be considered. To this end, a temperature-dependent asymmetric local free energy density for polymer crystallization has been given by Harrowell and Oxtoby,[21] that is,

$$f_{\text{local}}(\psi,T) = W \int_0^{\psi} \varphi(\varphi-\zeta)(\varphi-\zeta_0)\,\mathrm{d}\varphi$$

$$= W\left(\frac{\zeta\zeta_0}{2}\psi^2 - \frac{\zeta+\zeta_0}{3}\psi^3 + \frac{\psi^4}{4}\right), \quad (3)$$

where $\zeta = \zeta(T)$ corresponds to the unstable energy barrier, ζ_0 corresponds to the stable solidification potential, and W is a dimensionless coefficient describing the height of the energy barrier for surface nucleation. Here, ψ is limited between 0 and ζ_0. Therefore, ζ_0 may be regarded as the degree of crystal perfection. It may be simply evaluated as the ratio between melting temperature T_m and equilibrium melting point T_m^0 of a polymer crystal.[15]

As shown in Fig. 1, the local free energy density for a polymer melt generally satisfies the inequalities $f_\mathrm{local}(\zeta, T) > 0$ and $f_\mathrm{local}(\zeta_0, T) < 0$, hence there must be a $\hat{\psi}$ between ζ and ζ_0 at which $f_\mathrm{local}(\hat{\psi}, T) = 0$, i.e.,

$$W\left(\frac{\zeta\zeta_0}{2}\hat{\psi}^2 - \frac{\zeta+\zeta_0}{3}\hat{\psi}^3 + \frac{\hat{\psi}^4}{4}\right) = 0. \quad (4)$$

Solving ζ from Eq. (4), we have

$$\zeta = \frac{4\zeta_0\hat{\psi} - 3\hat{\psi}^2}{6\zeta_0 - 4\hat{\psi}}. \quad (5)$$

In Ref. [15], $\hat{\psi}$ is evaluated to be $\hat{\psi} = (T_\mathrm{m}^0 - T_\mathrm{m})/(T_\mathrm{m}^0 - T)$ according to the Hoffman and Weeks theory.[22] However, this evaluation cannot ensure $\hat{\psi} \le \zeta_0$, for example when $T = T_\mathrm{m}$, $\hat{\psi} = 1 \ge \zeta_0$. In this work, an alternative evaluation is given, that is,

$$\hat{\psi} = \frac{T_\mathrm{m}^0 - T_\mathrm{m}}{T_\mathrm{m}^0 - T}\zeta_0. \quad (6)$$

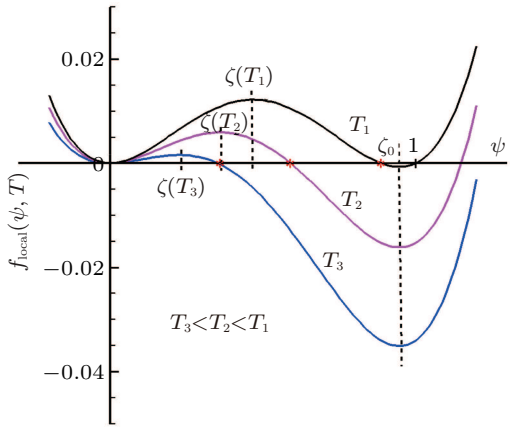


Fig. 1. (color online) Sketch map of local free energy density.

In addition, the nonlocal free energy density can be written in terms of the gradient of crystal order parameter describing the symmetric or asymmetric growth process as[15]

$$f_\mathrm{grad}(\psi) = \frac{1}{2}\kappa_0^2\beta^2(\theta)(\nabla\psi)^2, \quad (7)$$

where κ_0 is the coefficient of the interface gradient, $\beta(\theta)$ is a function of orientation angle θ, describing the anisotropic growth rate of the interface. In static crystallization, $\beta(\theta)$ is often given as

$$\beta(\theta) = 1 + \varepsilon\cos(j\theta), \quad (8)$$

where ε is the strength of anisotropy and j specifies the mode number. In phase field modeling, the orientation angle θ is defined as the angle between the interface normal and the reference axis, i.e.,

$$\theta = \arctan\left(\frac{\partial\psi/\partial y}{\partial\psi/\partial x}\right) = \arctan\left(\frac{\psi_y}{\psi_x}\right). \quad (9)$$

Substituting Eqs. (2), (3), and (7) into Eq. (1), one obtains

$$\begin{aligned}
&\frac{\partial\psi(\boldsymbol{x},t)}{\partial t} \\
&= -\Gamma\frac{\delta F(\psi)}{\delta\psi(\boldsymbol{x},t)} \\
&= -\Gamma\left(\frac{\partial f_\mathrm{local}(\psi,T)}{\partial\psi} - \frac{\kappa_0^2}{2}\nabla\cdot\left(\frac{\partial}{\partial\psi_x}\left(\beta^2(\theta)(\nabla\psi)^2\right)\right.\right. \\
&\quad \left.\left. + \frac{\partial}{\partial\psi_y}\left(\beta^2(\theta)(\nabla\psi)^2\right)\right)\right) \\
&= -\Gamma\left(W\psi(\psi-\zeta)(\psi-\zeta_0) - \kappa_0^2\nabla\cdot\left(\beta^2(\theta)\nabla\psi\right)\right. \\
&\quad + \kappa_0^2\frac{\partial}{\partial x}\left(\beta(\theta)\beta'(\theta)\frac{\partial\psi}{\partial y}\right) \\
&\quad \left. - \kappa_0^2\frac{\partial}{\partial y}\left(\beta(\theta)\beta'(\theta)\frac{\partial\psi}{\partial x}\right)\right). \quad (10)
\end{aligned}$$

Formulas for calculating W and κ_0 as well as a modified expression of ζ will be given in Subsection 2.3.

2.2. Temperature field

Another important factor in polymer isothermal crystallization is the self-generated temperature field created by the liberation of latent heat. The latent heat could exert an appreciable effect on the growth of a crystal interface. To determine the temperature at the growing crystal fronts, a heat conduction equation may be deduced from the conservation law of enthalpy taking the form of

$$\rho C_p\frac{\partial T}{\partial t} = k_T\nabla^2 T + \rho\Delta H\frac{\partial\psi}{\partial t}, \quad (11)$$

where ρ, C_p, and k_T are density, specific heat capacity, and thermal conductivity, respectively. If we define thermal diffusivity $\alpha = k_T/(\rho C_p)$ and $K = \Delta H/C_p$, then Eq. (11) reduces to

$$\frac{\partial T}{\partial t} = \alpha\nabla^2 T + K\frac{\partial\psi}{\partial t}. \quad (12)$$

In reality, the heat diffusion is much faster than the solute diffusion, thus time scales of Eqs. (10) and (12) have considerable differences in magnitude. When physical values are used, it will cause an unbearable computational burden. So

we are constrained to using a greater diffusion coefficient D or a smaller thermal diffusivity α. In this work, we increase the diffusion coefficient to let the ratio α/D be between 0.1 and 1.0. This artificial approach has a similar effect to those used in other phase-field models, which broadens the interface thickness artificially.[4] It has been shown that these artificial approaches are not only qualitative, but also have predictive power.

2.3. Dimensionless form

In order to present the phase-field equation (10) and heat conduction equation (12) in dimensionless forms, the temporal and spatial variables are rescaled to $\tau = Dt/d^2$, $\tilde{x} = x/d$, $\tilde{y} = y/d$, and the temperature is rescaled to $U = (T - T_m)/(T_m - T_c)$. Here T_c is the experimental temperature of crystallization. With these dimensionless variables, the final governing equations can be represented in the following dimensionless form:

$$\begin{aligned}\frac{\partial \psi}{\partial \tau} &= -\Bigg(W\psi(\psi-\zeta)(\psi-\zeta_0) - \tilde{\kappa}_0^2\tilde{\nabla}\cdot\left(\beta^2(\theta)\tilde{\nabla}\psi\right) \\ &\quad + \tilde{\kappa}_0^2\frac{\partial}{\partial\tilde{x}}\left(\beta(\theta)\beta'(\theta)\frac{\partial\psi}{\partial\tilde{y}}\right) \\ &\quad + \tilde{\kappa}_0^2\frac{\partial}{\partial\tilde{y}}\left(\beta(\theta)\beta'(\theta)\frac{\partial\psi}{\partial\tilde{x}}\right)\Bigg), \qquad (13)\\ \frac{\partial U}{\partial\tau} &= \tilde{\alpha}\tilde{\nabla}^2 U + \tilde{K}\frac{\partial\psi}{\partial\tau}, \qquad (14)\end{aligned}$$

where

$$\tilde{\nabla} = \left(\frac{\partial}{\partial\tilde{x}}, \frac{\partial}{\partial\tilde{y}}\right), \quad \tilde{\kappa}_0^2 = \frac{\kappa_0^2}{d^2}, \quad \tilde{\alpha} = \frac{\alpha}{D}, \quad \tilde{K} = \frac{K}{T_m - T_c}.$$

In the present study, equations (13) and (14) are solved over rectangular domains Ω together with homogeneous Neumann boundary conditions $\partial\psi/\partial\tau = 0$ and $\partial U/\partial\tau = 0$ imposed on the domain boundaries $\partial\Omega$. Initially, several points are placed in the domain to serve as seeds for initialing solidification. Initial data of ψ are prescribed to be ζ_0 at seeds and 0 elsewhere. The initial data of U are prescribed to be -1 throughout the entire domain.

The model parameters W and κ_0 should be determined first of all. In practice, both parameters can be accessible through experimentally measurable quantities. These temperature-dependent parameters may be expressed as[15,16]

$$W = 6\frac{\Delta H}{RT\zeta_0^3}\left(\frac{T_m - T}{T_m^0}\right)\left(\frac{\zeta_0}{2} - \zeta\right)^{-1}, \qquad (15)$$

$$\kappa_0 = 6\frac{\sigma}{nRT}\left(\frac{2}{W}\right)^{1/2}, \qquad (16)$$

where ΔH is the latent heat, R is the gas constant, σ is the surface free energy per unit area, and n is the amount of polymer monomers per unit volume. Note that, when T tends to T_m, $\zeta_0/2 - \zeta$ is a second-order infinitesimal of $T - T_m$. Thus W will be infinite as T tends to T_m. To avoid this, ζ must be modified. In this work, by using the methods given in Refs. [20] and [23], ζ is modified as

$$\bar{\zeta} = \zeta\left[1.0 + \frac{2.0}{\pi}\arctan(kU)\right], \qquad (17)$$

where k is a dimensionless coefficient inversely proportional to the supercooling. In this work, it is simply evaluated to be $k = \tilde{K}$. Although the values of W and κ_0 are changed due to the variations of $\hat{\psi}$ and ζ, the formulas of the W and κ_0 remain unchanged. So, calculating the two model parameters still needs the material parameters. The modified phase field model inherits the polymer characteristics of the original model. In additon, the relationships between the changed model parameters and polymer properties are the same as the previous ones. Finally, it should be emphasized that W and κ_0 are supercooling-dependent, and thus any variation in the crystallization temperature would change their values. But for isothermal crystallization, they may be calculated by substituting the crystallization temperature T_c into Eqs. (15) and (16) with the original expression of ζ.

3. Results and discussion

The power of the proposed phase-field model in predicting various spherulite morphologies will be demonstrated in this section. A set of material parameters cited from Ref. [15] is used for our simulations of isotactic polystyrene (iPS) solidification. According to these values, a set of model parameters is computed and specified in Table 1. In practice, the degree of crystallinity, crystal morphology, and crystal imperfection for polymer solidification are strongly dependent on supercooling. Thus T_m may be dependent on the supercooling. However, its value is often not determined experimentally for each crystallization temperature. In this work T_m is estimated from T_c and T_m^0 in accordance with the Hoffman–Week approach.[22,24] This may allow obtaining the model parameters associated with other experimental temperatures.

To solve the model, a number of numerical methods[25] can be used. In our simulations, both the finite difference method and the finite element method are employed on a grid size of 512×512. The dimensionless temporal step size and spatial step size are fixed to be $\Delta\tau = 0.1$, $\Delta x = \Delta y = 1.0$. Because the results obtained by both methods are the same, only the results of the finite difference method are shown.

As is well known, supercooling has a great influence on the crystallization morphology and crystallization kinetics of polymers. However, supercooling is not the only determinant of crystallization morphology. It is quite common to obtain crystals with different shapes for the same polymer under the same supercooling,[1,2] which means that there must be other

Table 1. Set of thermophysical material data and model data used for the simulations of iPS at a given experimental temperature of 210 °C.

Symbol	Data set	Symbol	Relation	Data set
T_{m}^{0}[°C]	242	Γ[s^{-1}]	D/d^2	10^5
T_{m}[°C]	233	ζ_0[−]	$T_{\mathrm{m}}/T_{\mathrm{m}}^{0}$	0.96
T_{c}[°C]	210	W[−]	$6\frac{\Delta H}{RT\zeta_0^3}\left(\frac{T_{\mathrm{m}}-T}{T_{\mathrm{m}}^{0}}\right)\left(\frac{\zeta_0}{2}-\zeta\right)^{-1}$	10.69
ΔH[kJ/mol] (of C_8H_8 units)	9.4×10^4	κ_0^2[m^2]	$\left(6\frac{\sigma}{nRT}\right)^2\left(\frac{2}{W}\right)$	1.2×10^{-14}
C_p[kJ/(mol K)] (of C_8H_8 units)	1.8	α[m^2/s]	$k_T/(\rho C_p)$	6.58×10^{-8}
k_T[J/(msK)]	0.128	K[K]	$\Delta H/C_p$	47.6
σ[kJ/m2]	7.65×10^{-4}			
ρ[kg/m^3]	1.08×10^3			
d[m]	1.0×10^{-7}			
D[m^2/s]	1.0×10^{-9}			

factors, such as thermal history, chain conformation, thickness of polymer film, etc., influencing the crystallization morphology. In the proposed phase-field model, these influences are reflected together by the anisotropic parameters ε and j. At present, the quantitative relationships between anisotropy and these factors are unavailable. Thus the values of the anisotropic parameters are varied to determine their roles in forming the crystallization morphologies.

Figure 2 shows the crystallization morphologies obtained by the current phase-field model with anisotropy mode $j = 6$. It is evident that supercooling strongly affects the interface structure. At a shallow supercooling of 22 °C, the crystal presents a hexagonal shape with faceted fronts. As anisotropy strength increases, the growth velocity near the middle parts of the lateral edges slows down, and thus concave facets are observed. With crystallization temperature decreasing, the facets are no longer flat, and the interface structures change into dendrite-like snowflakes. In addition, the density of the branches (or secondary arms) increases as the supercooling becomes deeper. As can be seen, at a crystallization temperature of 180 °C, the space between branches is so small that the branches cannot be easily differentiated from each other. Another important phenomenon is that the global\average growth rate is obviously increased as the crystallization temperature becomes smaller. In addition, increasing the anisotropy strength also leads to the increase of the number of branches. However, this "increase" is seemingly different from that caused by reducing the crystallization temperature. In this case, the six major branches change slightly and thus the contours remain almost the same. More importantly, and different from the crystallization temperature, the anisotropy strength seems to have no effect on the global growth rate.

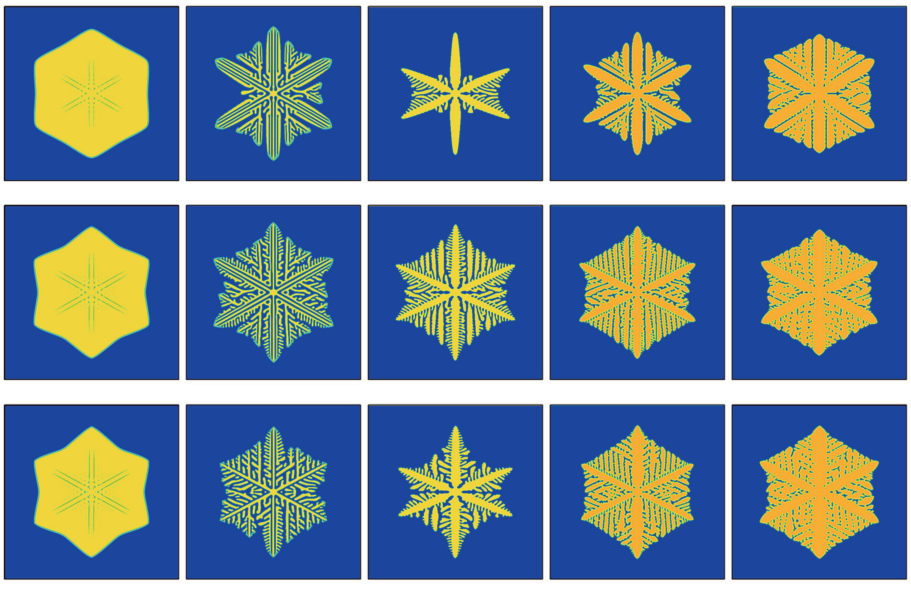


Fig. 2. (color online) Dendritic morphologies obtained at different crystallization temperatures with anisotropy mode $j = 6$, and anisotropy strength $\varepsilon = 0.01$, 0.03, 0.06 from top to bottom. (a) $T_{\mathrm{c}} = 220$ °C, $\tau = 320$; (b) $T_{\mathrm{c}} = 210$ °C, $\tau = 300$; (c) $T_{\mathrm{c}} = 200$ °C, $\tau = 250$; (d) $T_{\mathrm{c}} = 190$ °C, $\tau = 200$; (e) $T_{\mathrm{c}} = 180$ °C, $\tau = 180$.

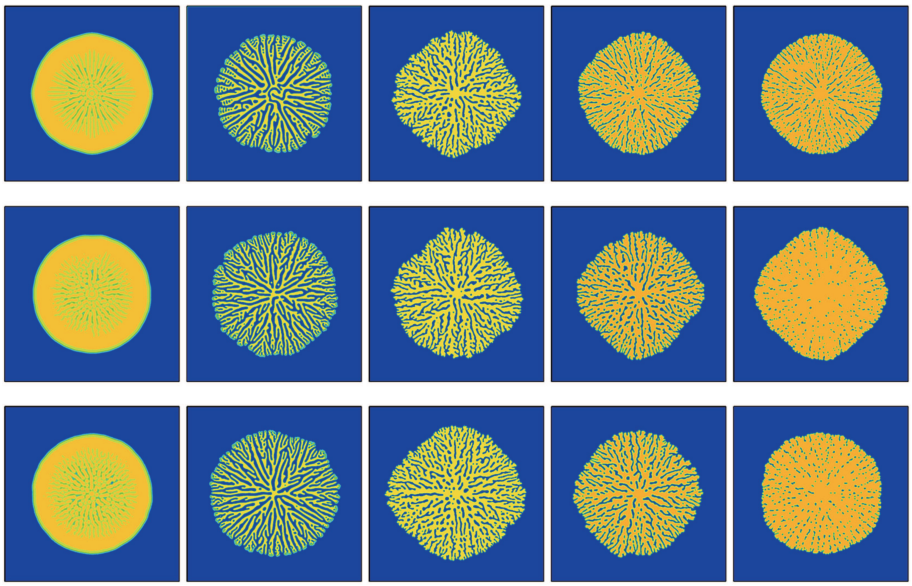


Fig. 3. (color online) Lamellar branching morphologies obtained at different crystallization temperatures with anisotropy mode $j = 36$, and anisotropy strength $\varepsilon = 0.01, 0.03, 0.06$ from top to bottom. (a) $T_c = 220$ °C, $\tau = 320$; (b) $T_c = 210$ °C, $\tau = 300$; (c) $T_c = 200$ °C, $\tau = 250$; (d) $T_c = 190$ °C, $\tau = 200$; (e) $T_c = 180$ °C, $\tau = 180$.

Next, to study the influence of the anisotropy mode on the crystallization morphology, a group of simulation results are shown in Fig. 3 with the anisotropy mode $j = 36$. Comparisons between Figs. 2 and 3 show that the interface structure is strongly affected by the anisotropy mode. At the shallow supercooling of 22 °C, the crystal presents a spherical shape with some internal structures. As crystallization temperature decreases, the interface structures change into dense lamellar branching morphologies (similar to seaweed). The branches in this case seem no longer rigid but soft. There are no obvious major branches. New branches are continuously generated from the sides of the existing branches, and eventually the dense lamellar branching morphologies are evolved. In this case, the effects of the crystallization temperature and anisotropy strength on the crystallization seem to be similar to those found in the dendritic case, so we will not repeat the analysis.

Dendritic morphology and lamellar branching morphology are two common categories observed experimentally during the solidification of iPS.[1,2] Besides, the ring-banded morphology can also sometimes be observed under certain conditions.[26] In the absence of anisotropy, the present phase-field model can be demonstrated to have the ability to simulate this structure in a narrow temperature range. Figure 4 shows some simulation results of the ring-banded morphology. At a temperature of $T_c = 212$ °C, an intact ring-banded structure is obtained. However, when the temperature is slightly changed, the stability of the structure will be reduced. Breakup of the ring-banded structure occurs when the crystal grows into a certain size. At a temperature of $T_c = 204$ °C, breakup occurs at a very early stage. The structure obtained is very similar to that with the lamellar branching morphology. Thus, breakup of the ring-banded structure is perhaps one of the potential ways to form the lamellar branching structure.

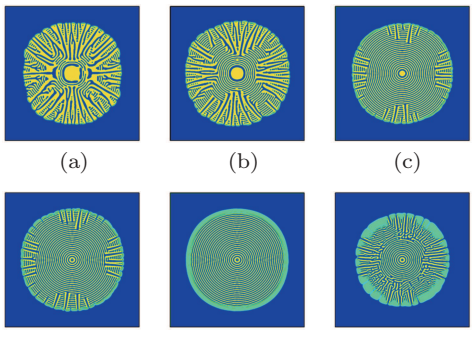


Fig. 4. (color online) Ring-banded morphologies obtained at different crystallization temperatures in the absence of anisotropy. (a) $T_c = 204$ °C, $\tau = 260$; (b) $T_c = 206$ °C, $\tau = 280$; (c) $T_c = 208$ °C, $\tau = 280$; (d) $T_c = 210$ °C, $\tau = 300$; (e) $T_c = 212$ °C, $\tau = 300$; (f) $T_c = 214$ °C, $\tau = 300$.

Furthermore, the ability of the present phase-field model to simulate multiple crystals is studied. In this case, the growth of each crystal may be restricted by its neighborhoods. Because the space is very limited for so many crystals, the crystal nuclei will be fighting each other for space to grow bigger. Once a growing crystal touches others, its growth velocity will slow down in the touching part but remain in the other part. Therefore, the shape of the crystal will become irregular and grain boundaries are formed between the touching crystals. Figure 5 shows some simulation results of the multiple crystals at a crystallization temperature of $T_c = 210$ °C. In these simulation cases, nine crystal nuclei are initially generated in the computational domain in a random way. As can be seen,

the grain boundaries between crystals are quite clear. They are straight in the isotropy case (ring-banded case) and nearly straight in the approximately isotropy case (lamellar branching case).



(a) (b) (c)

Fig. 5. (color online) Multiple crystals simulated at a crystallization temperature of $T_c = 210$ °C with different anisotropic parameters at $\tau = 200$. (a) $\varepsilon = 0$; (b) $\varepsilon = 0.03$, $j = 6$; (c) $\varepsilon = 0.03$, $j = 36$.

Finally, the computational cost of the present phase-field model is given. For the results at $\tau = 300$, the CPU times consumed by the finite difference method and the finite element method are about 220 seconds and 7200 seconds on an ordinary personal computer (CPU: AMD A6-3600, 2.10 GHz), respectively. Therefore, the present phase-field model is very highly efficient.

4. Conclusions

A phase-field model for simulating the spherulites of polymer melts is proposed by modifying the model proposed by Xu *et al.*[15] The new method inherits the virtues of Kyu's model, which includes obtaining its model parameters from the real material parameters and being very simple to use. It can reproduce various experimentally observed single crystal morphologies by employing a modified free energy functional form. Most importantly, the computational cost of the new model is greatly reduced. It allows for use on ordinary personal computers. A series of simulation results shows that the new model can reproduce morphologies of dendritic, lamellar branching, ring-banded , breakup of ring-banded, faceted hexagonal, and spherulitic structures. According to these results, it is clarified that supercooling and factors associated with anisotropy determine the morphology and microstructure of the crystal. Furthermore, it is confirmed that the global growth rate of the crystal (crystallization dynamics) is strongly dependent on supercooling but seems to be independent of anisotropy. Finally, simulation results for multiple crystals demonstrate the ability of the present phase-field model to reproduce the grain boundary. All the simulation results are qualitatively in accordance with experimental observations existing in the literature. However, there is still much work to be done for quantitative results.

References

[1] Taguchi K, Toda A and Miyamoto Y 2006 *J. Macromal. Sci. B* **45** 1141
[2] Bassett D C and Vaughan A S 1985 *Polymer* **26** 717
[3] Jin Y, Wang W and Su Z H 2011 *Appl. Spectrosc.* **65** 454
[4] Gránásy L, Pusztai T and Warren J A 2004 *J. Phys.: Condens. Matter* **16** R1205
[5] Ketdee S and Anantawaraskul S 2008 *Chem. Eng. Comm.* **195** 1315
[6] López J, Gómez P and Hernández J 2010 *J. Comput. Phys.* **229** 6663
[7] Raabe1 D and Godara A 2005 *Mater. Sci. Eng.* **13** 733
[8] Wendler F, Mennerich C and Nestler B 2011 *J. Crystal Growth* **327** 189
[9] Zaeem M A, Yin H and Felicelli S D 2012 *J. Mater. Sci. Technol.* **28** 137
[10] Gránásy L, Pusztai T, Tegze G, Warren J A and Douglas J F 2005 *Phys. Rev. E* **72** 011605
[11] Wu K A and Voorhees P W 2012 *Acta Mater.* **60** 407
[12] Kundin J, Siquieri R and Emmerich H 2013 *Physica D* **243** 116
[13] Chen C, Chen Z, Zhang J, Yang T and Du X J 2012 *Chin. Phys. B* **21** 118103
[14] Karma A and Rappel W J 1998 *Phys. Rev. E* **57** 4323
[15] Xu H J, Matkar R and Kyu T 2005 *Phys. Rev. E* **72** 011804
[16] Xu H J, Chiu H W, Okabe Y and Kyu T 2006 *Phys. Rev. E* **74** 011801
[17] Warren J A and Boettinger W J 1995 *Acta Metall. Mater.* **43** 689
[18] Kobayashi R, Warren J A and Carter W C 1998 *Physica D* **119** 415
[19] Wang D, Shi T F, Chen J Z, An L J and Jia Y X 2008 *J. Chem. Phys.* **129** 194903
[20] Kobayashi R 1993 *Physica D* **63** 410
[21] Harrowell P R and Oxtoby D W 1987 *J. Chem. Phys.* **86** 2932
[22] Hoffman J D and Weeks J J 1962 *J. Res. Natl. Bur. Stand. A* **66** 13
[23] Zhou D, Shi A C and Zhang P W 2008 *J. Chem. Phys.* **129** 154901
[24] Housmans J W, Peters G W M and Meijer H E H 2009 *J. Therm. Anal. Calorim.* **98** 693
[25] Wang X D, Ouyang J and Su J 2010 *Acta Phys. Sin.* **59** 6369 (in Chinese)
[26] Duan Y X, Zhang Y, Yan S K and Schultz J M 2005 *Polymer* **46** 9015